I.G. Boxx, O. Heinold, K.P. Geigle

Laser-induced incandescence measurements in a fired Diesel engine at 3 kHz

Published in Experiments in Fluids, 2015.
Volume 56, Issue 3, 2015. Article 3.

Original publication available at
http://link.springer.com/article/10.1007/s00348-014-1865-7
DOI: 10.1007/s00348-014-1865-7

Laser-induced incandescence measurements in a fired Diesel engine at 3 kHz

I.G. Boxx[1*], O. Heinold[2], K.P. Geigle[1]

1: Deutsches Zentrum für Luft- und Raumfahrt e.V., Pfaffenwaldring 38-40, 70569 Stuttgart, Germany
2: Robert Bosch GmbH, Robert-Bosch-Platz 1, 70839 Gerlingen, Germany
* corresponding author: Isaac.Boxx@dlr.de

Abstract Laser-induced incandescence (LII) was performed at 3kHz in an optically-accessible cylinder of a fired Diesel engine using a commercially available, diode-pumped solid state laser and an intensified CMOS camera. The resulting images, acquired every 3° of crank-angle, enabled the spatiotemporal tracking of soot structures during the expansion / exhaust stroke of the engine cycle. The image sequences demonstrate that soot tends to form in thin sheets that propagate and interact with the in-cylinder flow. These sheets tend to align parallel to the central axis of the cylinder and are frequently wrapped into conical spirals by aerodynamic swirl. Most of the soot is observed well away from the cylinder walls. Quantitative soot measurements were beyond the scope of this study but the results demonstrate the practical utility of using kHz-rate LII to acquire ensemble-averaged statistical data with high crank-angle resolution over a complete engine cycle. Based on semi-quantitative measures of soot distribution, it was possible to identify soot dynamics related to incomplete charge-exchange.

This study shows that long-duration, multi-kHz acquisition-rate LII measurements are viable in a fired Diesel engine with currently available laser and camera technology, albeit only in the expansion and exhaust phase of the cycle at present. Furthermore, such measurements yield useful insight into soot dynamics and therefore constitute an important new tool for the development and optimization of Diesel engine technology.

1. Introduction

Compression ignition Diesel engines are an efficient and widely used technology in the transportation industry. Increasingly strict regulation of both nitric-oxide (NOx) and soot emissions from Diesel engines has led to a number of innovations in engine technology, including new injector- and piston geometries, injection strategies, exhaust gas recirculation and swirl-enhanced in-cylinder mixture preparation. The complex mixture-preparation and combustion strategies on which these new technologies rely depend strongly upon a deep fundamental understanding of the physical processes relating to soot formation, agglomeration, breakup and oxidation.

Laser-based imaging diagnostics such as laser-induced incandescence (LII) are a key tool in understanding in-cylinder soot dynamics [1, 2]. In the LII measurement technique, soot particles are rapidly heated to ≥4000K using a high-intensity pulsed laser and the resulting incandescence is captured on a photo-sensor, typically a photomultiplier tube or an intensified camera. The LII technique can produce both point and planar, in-situ measurements of soot volume fraction and particle size. It has been used to study soot distributions in laboratory-scale test flames [3, 4], automotive engines [5–7], high-pressure combustors [8–10] and engine exhausts [11, 12]. A thorough review of the LII technique can be found in [13, 14].

A key limitation of LII stems from its need for high-intensity pulsed laser illumination which has, until recently, restricted it to temporally uncorrelated, single-shot or short-burst [15] measurements. While useful for studying mean quantities, temporally uncorrelated data is of limited utility in understanding the dynamic and spatiotemporally unpredictable processes that govern soot dynamics in a turbulent flame. The consequences of this limitation are particularly severe when LII is applied in a Diesel engine, where cyclic variations in fuel-air mixing, exhaust gas recirculation and flow-field turbulence lead to dramatic variation in soot dynamics from one cycle to the next. A thorough fundamental understanding of the dynamic processes that govern soot formation and oxidation in such a system clearly requires the ability to track soot structure and dynamics throughout individual engine cycles.

A second (and very practical) implication of the low acquisition rate of conventional, 10Hz, LII is that it makes it difficult and expensive to acquire crank-angle resolved statistics on soot dynamics. Degradation of the optically-accessible combustion liner and/or piston by soot in a research engine limits the number of

firing cycles one may accomplish in a given experiment before having to stop, open the engine and clean or replace the optical components. This places a clear premium on being able to collect as many measurements in a given firing cycle as possible.

The recent development of diode-pumped solid state (DPSS) lasers and intensified CMOS cameras with multi-kHz acquisition rates has enabled researchers to acquire LII measurements at much higher frame rates than was previously possible. Köhler et al. [16] used this technology to acquire simultaneous LII and particle image velocimetry (PIV) measurements of soot dynamics in a turbulent jet flame at 3kHz, over periods of 0.7s. These frame-rate and measurement durations are sufficient to resolve moderate- to large-scale turbulence-flame interactions in a typical Diesel engine over several complete engine cycles and may, therefore, be of considerable utility in understanding its soot dynamics. Acquiring such measurements in a fired Diesel engine, however, poses significantly greater technical challenges than those seen in [16]. These include distortion caused by imaging the measurement plane through a thick glass cylinder wall or piston head, first-surface reflections and window fouling. Signal quality may also be adversely affected by the intense background luminosity present during engine firings and by blockage or absorption of the LII signal before it reaches the camera in an effect known as “signal trapping”. Given the low pulse energy achievable with current-generation, kHz-rate DPSS lasers it is unclear whether long-duration, kHz rate LII measurements are feasible in a fired Diesel engine.

This study was designed to test the viability of acquiring usable LII measurements at multi-kHz acquisition rates in a fired Diesel engine with current-generation DPSS laser technology. The results are unique, in that they represent, to the authors’ knowledge, the first long-duration time-resolved measurements of soot dynamics in a fired Diesel engine using the LII measurement technique. The results provide unique insight into the processes governing soot dynamics and deeper statistical quantification of previously observed soot phenomena.

2. Experimental Details

2.1 Engine

The experiments were conducted in an optically accessible, compression-ignition Diesel. The design and operational parameters of the optically accessible engine (OAE) are described in Table 1. It is based on a production series four cylinder Diesel engine with an 84mm bore and 90mm stroke. Only one of the four cylinders is operational in this engine. Secondary gas mixtures (consisting of nitrogen, carbon dioxide and air) are supplied from a temperature-controlled, external reservoir to simulate exhaust gas recirculation.

Optical access in this engine is achieved through the quartz cylinder sleeve and (via a turning mirror) through a glass piston head. In the present study a top-hat profile piston geometry was used (rather than the more typical omega-shaped) with identical bowl volume in order to maintain the compression ratio. The top-hat piston profile also significantly eases the LII imaging requirements compared to those of an omega-shaped piston bowl by reducing laser reflections and image distortion. We note that modification of the piston-bowl shape necessarily alters the in-cylinder flow dynamics and care must be taken in interpreting the results as representative of different geometries. Sealing and lubrication of the piston is realized by oil-free, graphite piston rings.

Window fouling was a key limiting parameter in this study. The piston runs dry in the heated cylinder liner to avoid oil fouling of the optical components, but soot-buildup on the cylinder wall and piston limited the number of engine firings in a given image-acquisition run to approximately fifty. To ensure reproducible initial- and boundary-conditions for each firing, the engine was actively heated and motored for at least one minute at its operational frequency (1500rpm) prior to image acquisition. The engine was then fired at a cyclic rate of 1Hz (or every 14th cycle of the 4-stroke engine), which ensured stable resetting of the camera start trigger.

2.2 LII System

The kHz-LII imaging system is shown schematically in Figure 1. It consists of two main components, the excitation system and the imaging system. Each are described separately below.

2.2.1 Excitation System

The LII excitation system is based on a Q-switched, frequency-doubled DPSS (Nd:YAG) laser (Edgewave IS-8IIE) with an average power of 16.5W, or 5.5mJ/pulse at 3kHz and pulse-duration of 8.5ns. Although it is

common to use the fundamental (1064nm) wavelength of an Nd:YAG laser for LII and thereby avoid interference from fluorescence of polycyclic aromatic hydrocarbons (PAH), that was not possible in this experiment as the doubling-crystal is permanently mounted and sealed into this laser. Nonetheless, it is expected that laser-induced signal is dominated by soot (LII) over PAH (LIF) as the LII filter at 450 nm, i.e. blue-shifted from the excitation wavelength, is unfavorable for significant fluorescence. The laser produces a rectangular shaped beam with a top-hat intensity profile. A slight misalignment of the transmission optics at the output coupler of the laser results in a pattern of low-intensity interference fringes alongside this beam. These fringes were blocked with a rectangular aperture. A continuously variable beam attenuator consisting of a half wave plate and a polarizing beam-splitter cube was mounted at the exit of the laser to facilitate beam alignment with the laser operating at full power.

Two imaging configurations were implemented in this study. In the first configuration, the laser sheet was aligned to the vertical axis of the optically accessible engine (OAE) cylinder (i.e. oriented parallel to the direction of piston travel). In the second configuration, the laser sheet was oriented parallel to the piston head. In both configurations, the beam was formed into a thin sheet using a cylindrical lens (f1 = 1000mm) and focused to a waist using a spherical lens (f2 = 1000mm) and directed through the optically-transparent cylinder of a single-cylinder compression-ignition Diesel engine via turning mirrors. The same sheet-forming optics were used for both configurations, albeit with one additional turning mirror to rotate the orientation of the laser sheet.

The resulting laser sheet is estimated to be 6.5mm tall and 0.7mm thick at the probe volume, based on burn-marks taken on photographic paper. Although photographic burn paper can have a highly non-linear response, the estimated sheet thickness is consistent with that measured in Köhler et al. [16] using the same technique. Ensemble-averaged images of LII signal measured in the test volume indicate the beam profile had a uniform, top-hat profile across the height of the laser sheet while the perpendicular profile cannot be characterized in detail based on the burn-marks. For the sake of clarity though, subsequent discussion is limited to pulse energy, rather than laser fluence. Burn-marks taken with and without the glass-cylinder in the laser sheet showed no measureable difference in sheet thickness.

In contrast with other kHz repetition-rate laser diagnostic techniques (e.g. OH-PLIF), LII is not entirely non-intrusive. Depending on flow and chemical time-scales, individual soot particles may be exposed to multiple

LII excitation pulses. Onset of soot surface vaporization occurs close to the LII threshold of the so-called LII response curve and continues in the plateau region and towards higher fluences. The effect of enhanced soot sublimation resulting from soot particles being hit multiple times by the high repetition-rate laser has been addressed in one of our previous papers [16], where it was shown that the fluence of the LII excitation sheet was not higher than twice the apparent onset of the plateau region in the LII response curve. Vander Wal [18] found that fluences twice the onset of the soot threshold (being 0.3 J/cm^2 in his 1064 nm experiments) can result in mass losses of 20-25%. Losses of this magnitude are not observed in the sequences studied in detail, suggesting that bulk convection and through-plane swirl during the exhaust stroke minimize the occasions of individual soot particles being hit multiple times by the excitation later, yet maintaining structural features of the soot filaments. Therefore, the effect of significant laser-induced soot sublimation is not expected to affect our general findings.

2.2.2 Imaging System

LII emission was imaged with a highspeed, intensified CMOS camera aligned perpendicular to the laser beam. The camera, (LaVision HSS5) has a 10-bit dynamic range, 1024 × 1024 pixel imaging array. The camera was equipped with an external two-stage, lens-coupled image intensifier (LaVision HS-IRO) and a 100mm, f/2.8 (Tokina) objective lens. In the first imaging configuration, LII images were acquired through the optically-transparent engine cylinder. In the second configuration, wherein the laser sheet was oriented parallel to the piston head, images were acquired via reflection off an aluminum mirror mounted below the glass piston of the OAE. Elastic scattering from soot particles at 532nm (the excitation laser wavelength) was blocked using a band-pass interference filter (LOT-450 FS40-50) centered at $\lambda = 458 \pm 18$nm (FWHM). Background flame luminosity was minimized (to the extent possible) using a 100ns intensifier gate. The intensifier gate was prompt with respect to the laser pulse in order to maximize LII signal collection. The camera was equipped with 2.6GB of onboard memory, sufficient for 2048 full-frame images. Given the 6.5mm sheet height and 84mm cylinder diameter, the camera was operated in partial-frame mode, with a 1024×256 pixel area field of view.

In this study, LII imaging was accomplished during the expansion/exhaust stroke of the firing cycle. Intense background luminosity prevented the acquisition of usable LII measurements during the combustion phase

of cycle. This effect may be minimized in future studies through the use of an image intensifier with a gate-duration shorter than the 100ns (minimum) achieved in this study. At the 1500rpm frequency of the engine, one LII image was acquired for every 3° of engine crank-angle. Therefore, the onboard camera memory was segmented into 50 blocks of up to 163 frames each. Imaging sequences were triggered 36, 34 or 14° (depending on the operating condition) before the start of the expansion stroke of a firing cycle. The dynamics of the OAE made it impossible to synchronize the LII system directly with the engine to within the 100ns accuracy required by the intensifier gate. The camera and excitation laser were therefore operated at constant frequency using a digital delay generator (Quantum Composers Model 9528) as the master clock. The start of each (163-frame) LII image sequence was triggered by a TTL pulse generated by the OAE control system. Upon receiving this TTL start-trigger, the camera control unit (LaVision HSC) would begin image acquisition with the following cycle of the system master clock. The inability to directly synchronize the engine to the camera results in a timing jitter in the start trigger of an imaging sequence of 1/3000th of a second, or ±1.5° crank angle at the operational speed of the engine. It is important to note however, that this jitter affects only the start trigger of the run and results in a uniform timing offset throughout each 163-frame imaging loop. The activation time of the intensifier gate was monitored via a data-acquisition board and stored with the engine operational parameters.

3. Data Processing

3.1 LII Response Curve

Accurate interpretation of LII data depends on knowing the response characteristics of the measurement system. This is typically determined by measuring a response curve of the LII system in a well-defined sooting flame. Conventional LII imaging systems are usually operated in the so-called ‘plateau region’ of such a response curve [13, 17]. In this region the integrated LII signal measured by the detector becomes almost independent of the fluence of the excitation laser.

The small volume of the OAE cylinder and the lack of ventilation therein made it impossible to establish a stable, well-defined sooting flame in the imaging region of the LII system used in this study. As such, the

response curve was not measured directly in the present study. We note however, that the LII system used in the present study is almost identical to that implemented in an earlier study [16], wherein the response curve was measured. In that study the same laser and imaging optics were used to generate a laser sheet 6mm tall × 0.5mm thick, which closely resembles the 6.5mm × 0.7mm sheet used in the present study. The same imaging system, objective lens and filter were used in both studies. We note that the measurement conditions are not identical, in that Köhler et al. [16] studied flames of ethylene at atmospheric pressure while those studied in the present work were Diesel-fuelled and measured at slightly higher than atmospheric pressure. Köhler et al. [16] report reaching the plateau region of the LII response curve at a pulse-energy of 1.7mJ. Assuming a similar beam profile, one concludes the plateau region of the LII curve in the present study should be reached at pulse-energy of ≈ 2.54mJ. Accounting for decreased laser fluence due to first-surface reflection of the laser sheet as it passes through the OAE cylinder wall (≈ 7.7%), this figure increases to ≈ 2.75mJ. As the LII images in the present study were acquired at pulse-energies of 5.5mJ, it is reasonable to conclude that they, too, were in the plateau region of the LII response curve as visualized in the response curve in [16] where the LII signal does not change significantly upon variation of pulse energies between onset of the plateau region and twice that value.

3.2 Image Corrections

The LII images were first corrected for imaging system sensitivity. This was accomplished by computing the ensemble average of 2000 frames of a uniformly illuminated featureless white target (Kaiser Slimlite). Each LII image was then normalized with this ensemble-averaged image to correct for imaging system sensitivity. The effect of this sensitivity normalization was minor, resulting in approximately ±10% adjustment of intensity across the image. Distortions resulting from imaging through the curved glass cylinder of the OAE were eliminated by imaging a planar calibration target and de-warping the images according to a pinhole camera model. The de-warping algorithm used was implemented into a commercial image acquisition/analysis package (LaVision Davis 7.2). The axes of the de-warped images were then shifted such that their origins correspond to the centerline and top of the cylinder. The effect of the image de-warping and axis-mapping procedure is demonstrated in Figure 2. In the second imaging configuration (wherein the laser sheet was aligned parallel to the piston head) the grid target was imaged at each of the four laser sheet

heights, and the images de-warped accordingly.

3.3 Image Assessment

As the LII response curve was not measured directly, quantitative measurements of soot parameters such as concentration are beyond the scope of the present study. Nonetheless, several semi-quantitative measures of soot structure and distribution were extracted from the images for statistical characterization. Despite their semi-quantitative nature, the resulting statistical data yields useful insight into both the measurement technique and in-cylinder soot dynamics.

To extract these data, the LII images were cropped to the size of the laser sheet and then binarized according to a user-defined intensity threshold. The same intensity threshold was used for all runs. Using binary image labeling, each contiguous region of LII signal was identified. The resulting data was then filtered to leave only those regions with diameters greater than 3 pixels, or 0.25mm. The remaining data represents areas of LII signal above the detection limit of the kHz imaging system. This semi-quantitative data was then analyzed to compute statistical quantities including mean number density, area and spatial distribution of regions containing detectible LII signal. In addition, the binarized images were applied as masks to the (unthresholded) LII images to determine the mean brightness of these regions in the original image.

4. Results and Discussion

4.1 LII Signal vs. Flame Luminosity

Figure 3 shows three representative images acquired with the kHz-LII imaging system. The upper image was acquired during the combustion phase of the firing cycle, 24° after TDC. The middle image was acquired 48° after TDC, immediately after combustion is complete. The lower image was acquired during the exhaust phase of the cycle, 321° after TDC. It is clear from this figure that the background flame luminosity during the combustion phase of the cycle was significantly more intense than the LII signal. In fact, comparison of both single-shot and ensemble-averaged data at a given crank-angle suggests the background flame luminosity was at least an order of magnitude greater than the LII signal during the combustion phase of the

engine cycle. This likely results from two factors; 1) the relatively long (100ns) minimum integration time of the intensified camera and 2) the weak signal levels achieved during this phase of the cycle due to strong absorption of both the laser sheet and the resultant LII signal by in-cylinder soot particles. Although it is possible to subtract the mean background luminosity from single-frame or ensemble-average images acquired with the LII system, it was not possible to distinguish background luminosity from LII signal on a shot-by-shot basis during the combustion phase of the measurement. Subsequent discussion and analysis is therefore limited to LII measurements acquired in the post-combustion (expansion and exhaust) phase of the engine cycle.

4.2 Tracking soot structures

Figure 4 shows a series of images acquired via side-on imaging through the engine cylinder wall during the exhaust stroke of a single firing cycle. The firing cycle shown in Figure 4 was chosen for its high LII signal intensity but is otherwise representative of phenomena observed in the majority of LII acquisition sequences. Figure 4 shows each frame of a single measurement sequence, corresponding to 0.33ms or 3° crank-angle between the images. The sequence begins at crank angle position 214°, i.e. during the exhaust stroke of the engine cycle. Consistent with Figure 3, the illuminated region of each frame corresponds to the area excited by the laser sheet. Figure 4 reveals a number of important features on both the kHz-LII measurement technique and the in-cylinder soot dynamics.

It is clear from Figure 4 that the 3kHz acquisition rate of the LII system is sufficient to capture the dynamics of medium- to large-scale soot structures in the engine. In Figure 4, we observe what appear to be several large, spatiotemporally contiguous soot structures pass through the illuminated region from bottom to top. These structures consist of several thin layers that appear to convect and spatiotemporally evolve as they pass through the laser sheet. As each structure is observed to persist, largely intact, over the several frames it takes for them to pass through the measurement volume, it is reasonable to conclude the lifetime of these structures is on the order of that of the expansion / exhaust stroke or longer. Detectable quantities of soot are observable in the piston bowl as late in the cycle as 331° past TDC. The majority of the soot concentration in this sequence is observed on the right side of the image and appears to move up and to the right in the direction of the exhaust valve as it propagates through the measurement volume. Without simultaneous

planar velocimetry measurements, it is difficult to rigorously judge the relative influence of through-plane convection (induced by aerodynamic swirl about the cylinder centerline) on this apparent motion. Estimates based on cylinder geometry and engine rpm indicate fluid elements convect through the laser sheet height within four laser shots. This is consistent with the soot-structure dynamics observed in Figure 4. It is important to note too, that despite the peak laser-sheet fluence being approximately double that expected for the onset of soot sublimation, significant loss of material from the large-scale soot structures from one frame to the next is not observed. This suggests that, although the soot structures are spatially contiguous, individual soot particles are seldom hit more than once by a laser pulse (see discussion on this issue in section 2.2.1). Taken together, Figure 4 suggests that post-combustion oxidation of the soot was not efficient in this firing cycle and may have resulted in a significant concentration of soot leaving the cylinder with the exhaust. Although the reason for this is not clear from the LII images alone, the ability to spatiotemporally track dynamics like these represents a new experimental capability for helping understand such phenomena.

Figure 5 shows a representative image sequence acquired (via a turning mirror) through the piston bowl. In this measurement, the laser sheet was oriented parallel to the piston head. As before, it shows each frame of an imaging run, beginning at 214° after TDC. This image sequence was chosen for display due to its high soot concentration, but is otherwise characteristic of the phenomena observed in this study. In Figure 5 we observe a spiral-shaped soot structure that appears to grow in overall diameter and soot concentration and then shrinks again with increasing time. The center of this structure does not show significant left-to-right movement in the image. Given the mean through-plane velocity induced by the traveling piston, it is reasonable to conclude the image sequence in Figure 5 shows a soot structure being wrapped into a spiral-shape under the influence of a swirl-induced vortex with a rotation axis oriented approximately parallel to the cylinder centerline.

Although acquired separately, it is instructive to compare the image sequences in Figs. 4 and 5. Whereas the soot structures observed in Figure 4 show mainly thin, sheet-like structures that appear to move up and to right with the bulk flow of gas in the cylinder, the soot structures observed in Fig. 5 show little left-to-right movement across the image. The growth and subsequent shrinkage of the vortex diameter is consistent with the strong left-to-right movement observed in Figure 4, as is the detectable quantity of soot remaining in the

piston bowl at 331° past TDC. The wrapping of a soot layer into a spiral-shaped structure is consistent with layering of thin soot sheets observed in Figure 4.

4.3 Highly-resolved statistics

The high cycle-to-cycle variation in soot concentration and distribution in a fired Diesel engine makes ensemble-averaging essential for the reliable interpretation of LII data. The technical challenge and high cost of operating an optically-accessible Diesel engine test stand impose a severe practical limitation on the number of points in a firing cycle where ensemble-averaging is feasible. Coarsely-resolved (with respect to crank-angle) statistics can obscure important physical phenomena. A key potential advantage of kHz-rate LII measurements is that they enable much more highly-resolved statistical data on soot dynamics.

Although quantitative measurement of soot concentration and particle size is beyond the scope of this study, Figure 6 demonstrates the utility of highly-resolved LII statistics in better understanding soot dynamics in a Diesel engine. Figure 6a shows the mean number of elements identified in the binary LII images, i.e. the number of regions in each image with detectable LII signal. The profile corresponds to the ensemble-average of (?) 350 engine cycles, acquired with 3° crank-angle resolution. The error bars correspond to ± 1σ (standard deviation). Figure 6b shows the mean area of these elements at each crank-angle position. Whereas Figure 6a and 6b show the number density and mean area of regions in the image with detectible LII signal, Figure 6c shows the ensemble average of the following quantity

$$\beta = \sum_{j=1}^{N} (\mathrm{A}_j \times B_j) \tag{1}$$

where A_j is the area of element j in the binarized LII image and B_j is the mean brightness of the corresponding area in the unthresholded LII image. We note that LII imaging is a two-dimensional technique which can dissect three-dimensional structures and may give the false impression of breaks in the soot sheet layer. One should exercise due caution to avoid interpreting this semi-quantitative statistical data over-broadly. Although not a quantitative measure of soot concentration, the quantity β yields qualitative insight into the relative LII signal at each measured crank-angle.

Taken together, the profiles in Figure 6 yield significant insight into the in-cylinder soot dynamics of this engine. After the initial image-saturation fades at ca. 60°, little LII signal is observed in the measurement volume until approximately 180°, at which point a steady rise in the number, size, and brightness of locations with particles is seen. This increase continues until ca. 270°, after which it fades back to approximately zero at 360°. A small dip in the profile is observable at 320-330°. This dip is a measurement artefact associated with the passage of the top edge of the glass piston passing through the measurement volume.

Of particular interest in Figure 6 is a rise in LII signal observable between 360° and 420°. This measurable rise in LII signal is indicative of the presence of soot in the cylinder during the intake stroke. This likely results from the fact that the intake valve of the engine opens before TDC, allowing some soot-containing gases to enter the intake line. After the exhaust valve closes, and the new charge is drawn in through the intake, the soot-containing gas is drawn back into the cylinder. Although this is not the first time this phenomenon has been observed, Figure 6 provides a convincing example of the ease with which such features are observable (and interpreted) when one has highly resolved statistics such as those presented here.

5. Conclusions

Laser-induced incandescence (LII) was performed at 3kHz in an optically-accessible cylinder of a fired Diesel engine using a commercially available, diode-pumped solid state laser and an intensified CMOS camera. The resulting images, acquired every 3° of crank-angle, enabled the spatiotemporal tracking of soot structures during the expansion / exhaust stroke of the engine cycle. The image sequences demonstrate that soot tends to appear in thin sheets that propagate and interact with the in-cylinder flow. These sheets tend to align parallel to the central axis of the cylinder and are frequently wrapped into conical spirals by aerodynamic swirl. The majority of soot is observed well away from the cylinder walls. Quantitative soot measurements were beyond the scope of this study but the results demonstrate the practical utility of using kHz-rate LII to acquire ensemble-averaged statistical data with high crank-angle resolution over a complete

engine cycle. Semi-quantitative measures of soot distribution yielded evidence of incomplete charge-exchange.

This study shows that long-duration, multi-kHz acquisition-rate LII measurements are viable in a fired Diesel engine, albeit only in the expansion and exhaust phase of the cycle at present. Furthermore, such measurements yield useful insight into soot dynamics and therefore constitute an important new tool for the development and optimization of Diesel engine technology.

References

1. A.C. Eckbreth, J. Appl. Phys. 48 (1977) 4473–4479.
2. L.A. Melton, Appl. Opt. 23 (1984) 2201–2208.
3. C.R. Shaddix, K. Smyth, Combust. Flame 107 (1996) 418-452.
4. S. Will, S. Schraml, A. Leipertz, Proc. Combust. Inst. 26 (1996) 2277-2284.
5. J.E. Dec, A.O. zur Loye, D.L. Siebers, SAE Technical Paper 910224, 1991.
6. B. Bougie, L.C. Ganippa, A.P. van Vliet, W.L. Meerts, N.J. Dam, J.J. ter Meulen, Combust. Flame 145 (2006) 635-637.
7. B.F. Kock, B. Tribalet, C. Schulz, P. Roth, Combust. Flame 147 (2006) 79-92.
8. M. Braun-Unkhoff, A. Chrysostomou, P. Frank, E. Gutheil, R. Lückerath, W. Stricker, Proc. Combust. Inst. 27 (1998) 1565-1572.
9. M. Hofmann, W.G. Bessler, C. Schulz, H. Jander, Appl. Opt. 42 (2003) 2052-2062.
10. O. Lammel, K.P. Geigle, R. Lückerath, W. Meier, M. Aigner, in Proc. ASME Turbo Expo 2007, Power for Land, Sea and Air, Montreal (Canada), 14.–17.05.2007 (2007). Paper GT2007-27902
11. D.R. Snelling, G.J. Smallwood, R.A. Sawchuk, W.S. Neill, D. Gareau, D.J. Clavel, W.L. Chippior, F. Liu, Ö.L. Gülder, SAE Tech. Paper 2000–01–1994. Society of Automotive Engineers, Warrendale, PA, 2000
12. J.D. Black, M.P. Johnson, Aerosp. Sci. Technol. 14 (2010) 329-337.
13. R.J. Santoro, C.R. Shaddix, in Applied Combustion Diagnostics, ed. by K. Kohse-Höinghaus, J. Jeffries (Taylor and Francis, London, 2002)
14. C. Schulz, B.F. Kock, M. Hofmann, H. Michelsen, S. Will, B. Bougie, R. Suntz, G. Smallwood, Appl. Phys. B 83 (2006) 333-354.
15. J. Sjöholm, R. Wellander, H. Bladh, M. Richter, P.E. Bengtsson, M. Alden, U. Aronsson, C. Chartier, O. Andersson, B. Johansson, SAE Int. J. Engines 4 (2011) 1607-1622.
16. M. Köhler, I. Boxx, K.P. Geigle, W. Meier, Appl. Phys B 103 (2011) 271–279.
17. P.O. Witze, S. Hochgreb, D. Kayes, H.A. Michelsen, C.R. Shaddix, Appl. Opt. 40 (2001) 2443-2452.
18. R.L. Vander Wal, T.M. Ticich, A.B. Stephens, Appl. Phys. B 67 (1998) 115-123.

Engine Characteristics and Operating Parameters	
Piston geometry	Top-hat bowl
Engine bore / stroke	84mm / 90mm
Compression ratio	16
Swirl ratio	1.8
Fuel injection system	Bosch Gen. III (Piezo)
Nozzle	7-hole
Rail pressure	525 bar
Fuel	Diesel (DIN EN 590)
Injection timing	Pilot: 12° before TDC
	Main: 1.5° after TDC
Intake pressure	1.38 bar
EGR Rate (synthetic mixture)	37%
Intake Mixture	80.2% N_2, 16.9% O_2, 2.9% CO_2
Engine speed	1500 RPM
Load (IMEP)	4.3 bar
Lambda	1.8

Table 1 - Engine Characteristics and Operating Parameters

List of Figure Captions

Figure 1 – Experimental setup and imaging configuration.

Figure 2 – Effect of image de-warping. Upper Image – Raw image. Lower Image – Corrected.

Figure 3 - Background flame luminosity vs. LII signal strength. Top = 24°, Middle = 48°, Bottom = 312° after TDC. Note the order of magnitude difference in colour bars.

Figure 4 – LII image sequence acquired via side-on imaging through the engine cylinder wall, with the laser sheet oriented parallel to the piston centerline axis. Each column represents 21° crank-angle, with each frame corresponding to 3° crank-angle.

Figure 5 – LII image sequence acquired via a turning mirror through the piston, with the laser sheet oriented parallel to the piston head. Each column represents 21° crank-angle, with each frame corresponding to 3° crank-angle.

Figure 6 – Statistical quantities extracted from kHz-LII measurements acquired during the exhaust stroke of the fired Diesel engine. a) Number of image elements with detectable LII signal. b) Mean area of image elements with detectable LII signal. c) Quantity β as defined in Eqn. 1.

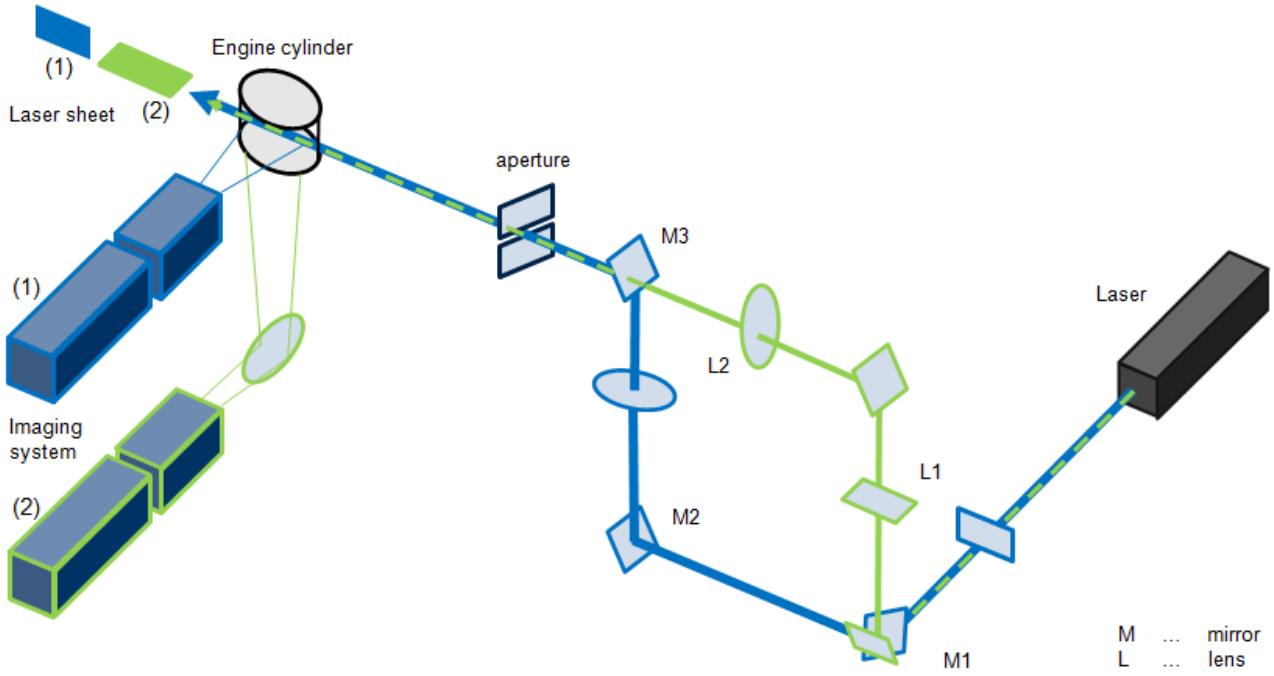

Figure 1 – Experimental setup and imaging configuration.

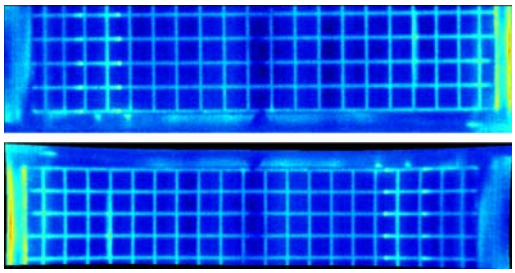

Figure 2 – Effect of image de-warping. Upper Image – Raw image. Lower Image – Corrected.

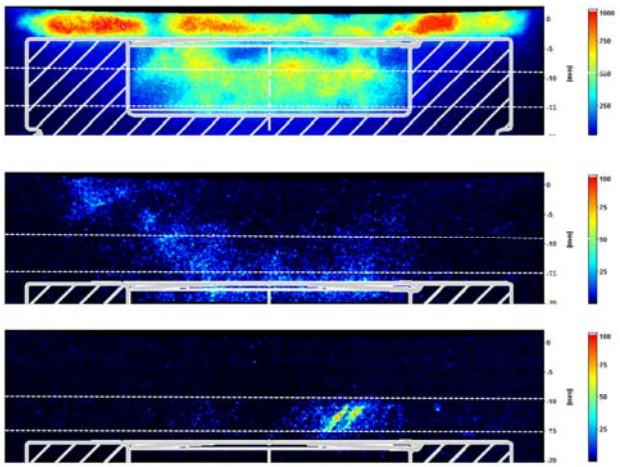

Figure 3 - Background flame luminosity vs. LII signal strength. Top = 24°, Middle = 48°, Bottom = 312° after TDC. Note the order of magnitude difference in colour bars.

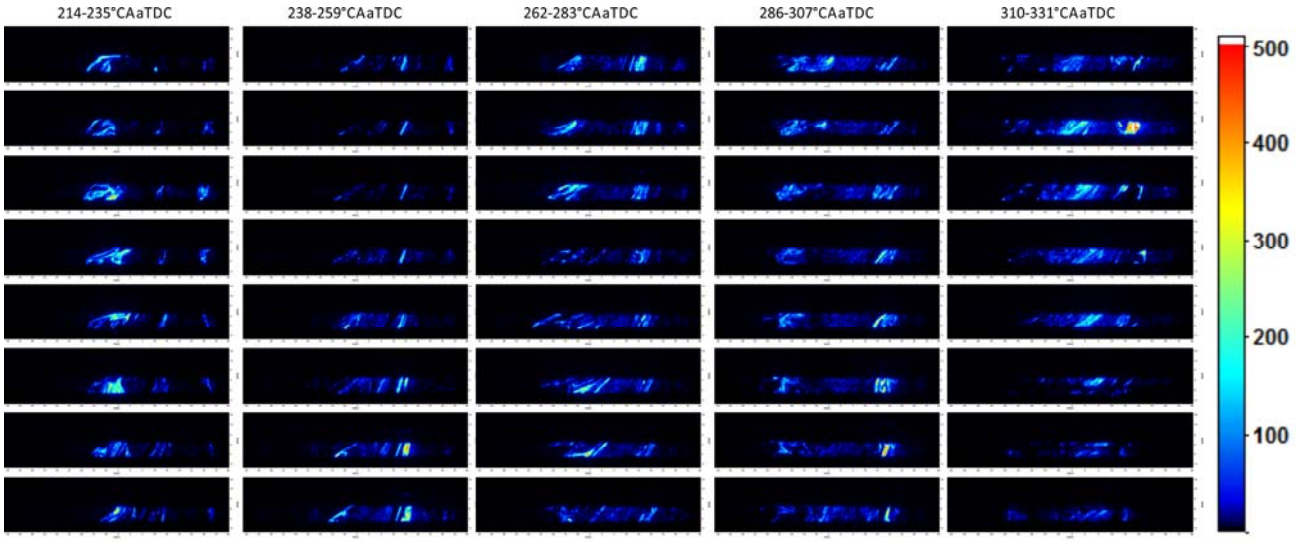

Figure 4 – LII image sequence acquired via side-on imaging through the engine cylinder wall, with the laser sheet oriented parallel to the piston centerline axis. Each column represents 21° crank-angle, with each frame corresponding to 3° crank-angle.

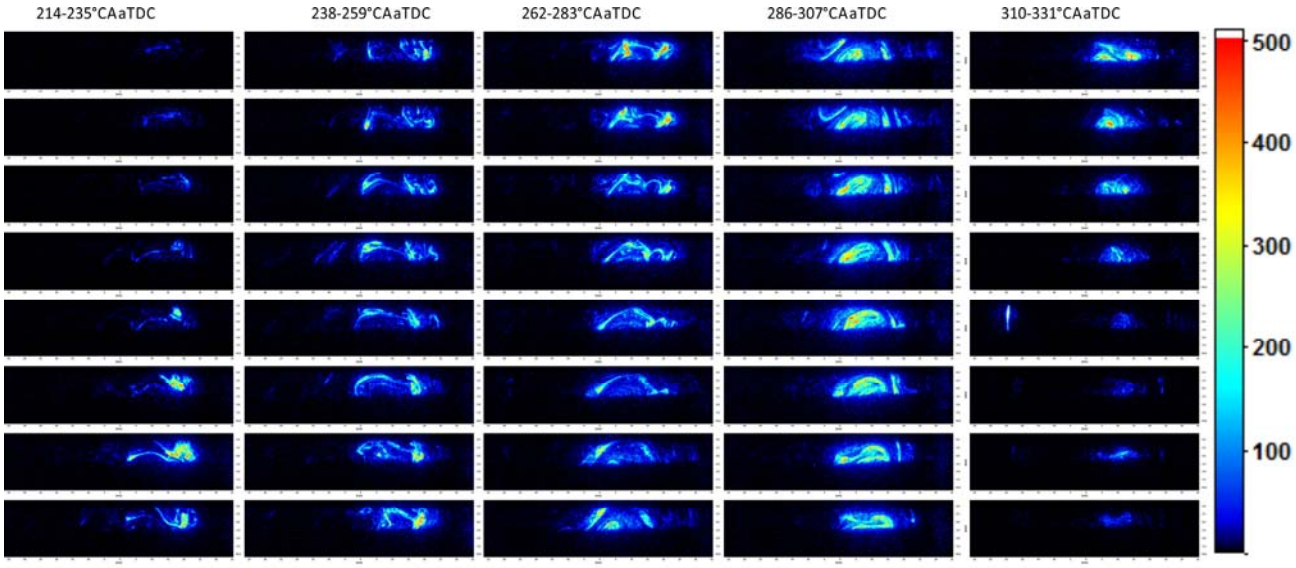

Figure 5 – LII image sequence acquired via a turning mirror through the piston, with the laser sheet oriented parallel to the piston head. Each column represents 21° crank-angle, with each frame corresponding to 3° crank-angle.

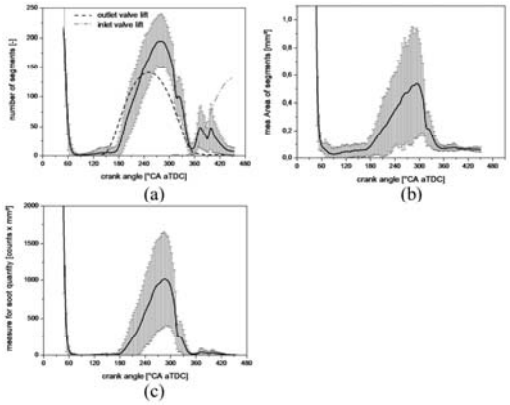

Figure 6 – Statistical quantities extracted from kHz-LII measurements acquired during the exhaust stroke of the fired Diesel engine. a) Number of image elements with detectable LII signal. b) Mean area of image elements with detectable LII signal. c) Quantity β as defined in Eqn. 1.